Scientific and Social Research, 2026, Volume 8, Issue 2
https://ojs.bbwpublisher.com/index.php/SSR
Online ISSN: 2981-9946
Print ISSN: 2661-4332

Design and Ultrafast Laser Direct Writing of Drag-Increasing Structures on Valve Surfaces

Hao Wang*, Yu Tan*

State Key Laboratory of Ultrafast Optical Science and Technology, Xi'an Institute of Optics and Precision Mechanics, Chinese Academy of Sciences, Xi'an 710119, Shaanxi, China

**Corresponding authors: Hao Wang, wanghao1@opt.ac.cn; Yu Tan, tanyu@opt.ac.cn*

Abstract: To address the issues of significant damping attenuation and short service life of existing drag-increasing valves, this study proposes a design and fabrication method for such valves based on recessed microstructures. The finite element method (FEM) was employed to simulate the effects of microstructural geometric parameters on gas flow pressure drop, and the optimal structural parameters were determined as follows: groove depth of 0.63 mm, bottom parameter of 0.66 mm, and base angle of 43.67°. Subsequently, a picosecond laser integrated with a power stabilization system was used to fabricate the microstructures on rotating workpieces, achieving a geometric accuracy better than 3 μm. Tests under actual operating conditions indicate that the drag of the processed workpiece is increased by approximately 50% compared with the unprocessed counterpart.

Keywords: Laser fabrication; Drag-increasing structure; Ultrafast laser direct writing; Finite element simulation

Online publication: March 18, 2026

1. Introduction

Drag-increasing valves are capable of regulating airflow velocity and have been widely applied in fields such as aerospace [1]. Existing drag-increasing methods primarily rely on adding O-rings to form local protrusions for drag augmentation. However, their damping performance attenuates significantly with an increasing number of valve actuation cycles, which compromises the service life of the valves. In this application scenario, concave structures offer a longer service life compared to convex structures. Previous studies have demonstrated that surface textured structures can regulate friction, and the drag regulation effect is directional, with this directionality correlated with the orientation of the textures (or microstructures) [2–4]. Based on these findings, this study designs a drag-increasing functional structure on the valve surface using groove structures and fabricates it on rotating parts via a picosecond laser equipped with a power stabilization system, thereby realizing the manufacturing of the designed structure.

2. Design

The FEM was adopted to simulate the drag-increasing functional structure. Considering the feasibility of practical fabrication, the structure was designed as V-shaped grooves. Given that the specimen has a rotating structure, it can be simplified to an axisymmetric 2D model. The geometric configuration under typical microstructure parameters is illustrated in **Figure 1a**, where the axis of symmetry is located at r = 0 on the left side. The blue region represents air, while the gray region denotes the specimen. The inner diameter of the air channel, determined by the rotating specimen, is 32.15 mm, with the outer diameter limited to 33.15 mm. In the shown polar coordinate system (r, z), the drag-increasing microstructure is a triangular area enclosed by three points, namely A (16.075 mm, 0), B (16.075 mm − deep, −b), and C (16.075 mm, −0.4 mm). Specifically, the groove width is 0.4 mm, the groove depth (deep) ranges from 0.23 mm to 0.63 mm, and the parameter b is used to control the bottom position of the microstructure. Considering the upper limit of typical conditions, the boundary conditions were set as follows: a constant mass flow rate of 5 g/s at the inlet (upper boundary), corresponding to an inlet flow velocity of approximately 100 m/s, and a static pressure of 0 Pa (i.e., equal to the ambient pressure of 0.2 MPa) at the outlet (lower boundary). The Reynolds number of the system under these operating conditions is approximately 7000. The simulation was performed using the CFD-Turbulence-SST (Menter Shear-Stress Transport) module in COMSOL Multiphysics. The SST method incorporates blending functions F_1 and F_2, which enable a smooth transition between the k-ω model and the k-ε model, while restricting shear stress to enhance the consistency of the simulation with actual conditions [5].

A typical mesh generation scheme is illustrated in **Figure 1b**, with additional refinement implemented in the vertical direction at the edges. Specifically, a total of 16 boundary layers were constructed near the main channel walls, where the thickness of the first layer was 0.5 μm, and each subsequent layer was increased by a factor of 1.2. In the microstructure region, where the fluid velocity is relatively low, the boundary layers were coarsened to 12 layers in total, with a first-layer thickness of 0.8 μm and a growth factor of 1.2 for each successive layer. The maximum element size of the remaining meshes was set to 112 μm. Under the aforementioned operating conditions and mesh configuration, the wall resolution was consistently below 0.5, indicating high computational accuracy.

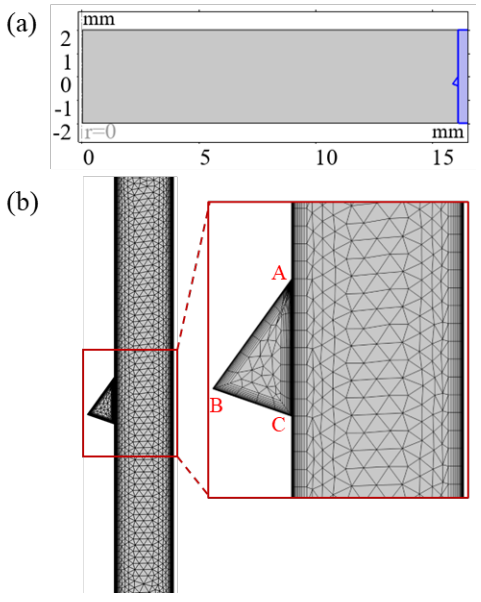

Figure 1. Finite element model setup of the drag-increasing structure: (a) Geometric configuration; (b) Mesh generation

The calculation process was divided into two steps. First, wall distance initialization was performed to obtain the distance from each cell to the nearest wall, thereby calculating the blending functions F_1 and F_2 and achieving a smooth transition between the near-wall and far-field models. Second, the distributions of other characteristic parameters of the flow field (e.g., velocity and pressure) were computed. The pressure drop characteristics under different base angle parameters (b, deep) were simulated, where deep ranged from −0.1 mm to 0.8 mm and b ranged from 0.23 mm to 0.63 mm.

A typical distribution of pressure and flow velocity is presented in **Figure 2a**. It can be observed that the airflow velocity inside the microstructure is significantly lower than that outside and decreases continuously with increasing microstructure depth, with the airflow primarily flowing near the top of the microstructure. The pressure gradient inside the microstructure is substantial and concentrated near the distal end of the microstructure (i.e., point C in **Figure 1**), exhibiting a maximum value. The relationship between the maximum pressure inside the microstructure and the structural parameters is illustrated in **Figure 2b**. It can be seen that the maximum pressure is mainly affected by the depth, decreasing essentially with increasing depth. When ∠A is an acute angle (i.e., b < 0), the maximum pressure value is relatively small.

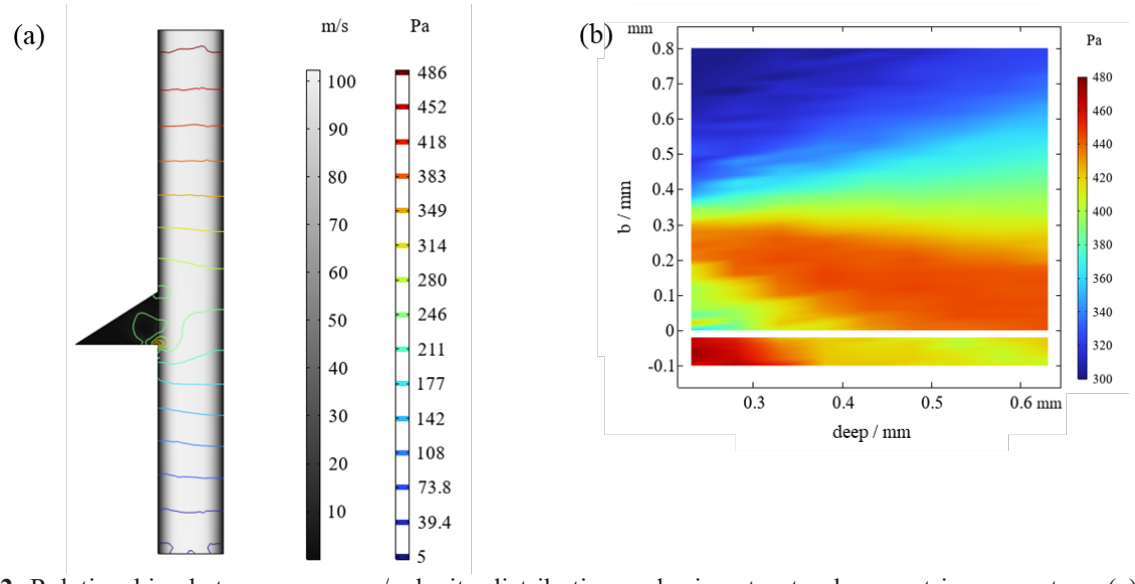

Figure 2. Relationships between pressure/velocity distribution and microstructural geometric parameters: (a) Overall situation under typical case (b=0.4 mm, deep=0.63 mm); (b) Relationship between the maximum pressure inside the microstructure and geometric parameters

The pressure drop characteristics under different structural parameters are illustrated in **Figure 3**, where the straight line at b=0.4 mm indicates that ∠C=90° at this point. The simulation results demonstrate that this structure exhibits an excellent drag-increasing effect; however, abrupt low points exist under certain conditions. When deep = 0.63 mm, the pressure drop reaches a relatively high value at b=0.66 mm, and the pressure drop levels in the adjacent range remain favorable. Therefore, the structural parameters at this point were selected as the fabrication target, corresponding to ∠A=43.67°.

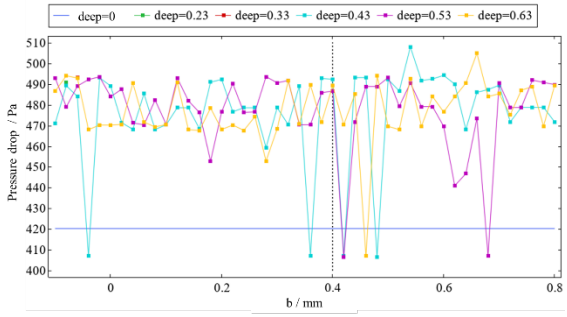

Figure 3. Influence of different structural parameters (b, deep) on pressure drop (the unit of deep is mm)

Fabrication experiments were conducted in accordance with the aforementioned simulation results. The laser system employed consisted of an Advanced Optowave laser (central wavelength: 1064 nm, pulse width: 12 ps, beam quality M^2<1.3) and a focusing system composed of an x, y- galvanometer scanner and an f-θ field lens. This focusing system had a focal length of 200 mm, resulting in a focused spot diameter of 30 μm. Since the complete fabrication of the specimen was quite time-consuming, the stability of the laser power was particularly critical. Thus, an additional laser power stabilization system was integrated to suppress power fluctuations. This system was mainly composed of a motor-driven rotatable half-wave plate, a Brewster mirror, a sampling mirror, and a power meter. It could perform real-time regulation of the laser power in the fabrication optical path based on the readings of the power meter, with the power stability after regulation reaching ±0.5%. The fabrication optical path is illustrated in **Figure 4**. The workpiece to be processed was a 05Cr17Ni4Cu4Nb rotating component with a diameter of 32.15 mm.

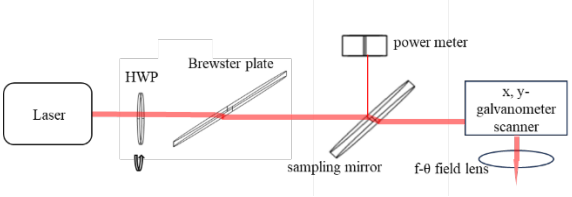

Figure 4. Schematic diagram of the fabrication optical path

The optimal range of single-pulse energy was determined to be 24–36 μJ via single-pulse experiments. On this basis, other fabrication parameters were adjusted to match the geometric shape predicted by the simulation results, and the optimal fabrication parameters were finalized as follows: the laser beam was incident at an angle of 55° relative to the fabrication surface, with a single-pulse energy of 30 μJ, a repetition frequency of 500 kHz, a scanning speed of 120 mm/s, a scanning interval of 10 μm, and a total of 12 scanning layers. The workpiece fabricated under these parameters is presented in **Figure 5**. A laser confocal microscope was utilized to characterize its three-dimensional morphology. Owing to the limitation imposed by its obtuse-angle structure, the workpiece was placed at an angle of 45° relative to the microscope stage during the scanning process, and the corresponding characterization results are illustrated in **Figure 5b** and **Figure 5c**. It was verified that the structural parameters of the fabricated workpiece were basically consistent with the simulation requirements. A photograph of the machined workpiece is shown in **Figure 5a**, with the geometric parameters (groove width and groove depth) of the machined area achieving a precision better than 3 μm. Tests conducted under actual working conditions demonstrated that, compared with the unprocessed workpiece, the drag of this machined workpiece was increased by approximately 50%.

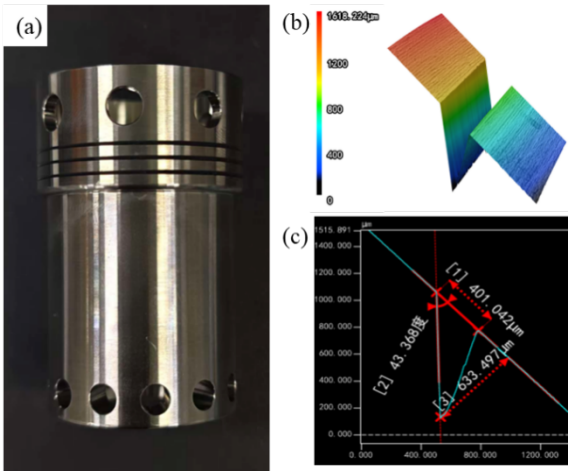

Figure 5. Processed workpieces: (a) Physical photos; (b) 3D morphology of microstructures; (c) Cross-sections of microstructures

3. Conclusion

This study proposes a design and fabrication method for drag-increasing valves with recessed microstructures. Through finite element simulation, the influence mechanism of the geometric parameters of V-shaped grooves on airflow pressure drop was systematically analyzed, and the optimal structural parameters were determined (groove depth: 0.63 mm, bottom parameter: 0.66 mm, base angle ∠A=43.67°). Subsequently, a picosecond laser equipped with a power stabilization system was adopted to successfully fabricate the microstructures on rotating workpieces, achieving a geometric accuracy better than 3 μm and a drag increase of approximately 50% under actual operating conditions. Experimental results demonstrate that the designed groove structures can effectively achieve the drag-increasing function, and this structural design provides a new approach to meeting the long-service-life requirements of valve damping.

Funding

This research was funded by the National Key Research and Development Program of China (2022YFB4602600) and the National Defense Basic Scientific Research Program of China (JCKY2023130C001)

Disclosure statement

The authors declare no conflict of interest.

References

[1] Kuang YW, Xu SJ, Fu LP, et al., 2025, Boosting Check Valve and Gas Boosting System for Gas Boosting System: CN202411441368.1.

[2] Song JZ, Li GY, 2024, Shape Optimization and Mechanism of Transverse Groove for Drag Reduction Based on Genetic Algorithm. Journal of Aerospace Power, 2024(5): 231–238.

[3] Li SC, Wu D, Cui GY, et al., 2020, Experimental Study on Properties of Turbulent/non-turbulent Interface over Riblets Surfaces at Low Reynolds Numbers. Chinese Journal of Theoretical and Applied Mechanics, 2020(6): 1632–1644.

[4] Li TT, Shen KY, Xiang C, et al., 2025, Hierarchical Wrinkled Structures via 3D Printing and Self-organization for Energy-efficient Transport. Matter, 8(12): 102345.

[5] Menter FR, Kuntz M, Langtry R, 2003, Ten Years of Industrial Experience with the SST Turbulence Model. Heat and Mass Transfer, 2003(4): 1–8.